

1 **Accelerated Estimation of Sea Spray-Mediated Heat Flux**  
2 **Using Gaussian Quadrature: Case Studies with a Coupled**  
3 **CFSv2.0-WW3 System**

4 Ruizi Shi<sup>1</sup> and Fanghua Xu<sup>1\*</sup>

5 <sup>1</sup> Department of Earth System Science, Ministry of Education Key Laboratory for Earth System  
6 Modeling, Institute for Global Change Studies, Tsinghua University, Beijing, 100084, China.

7 *\*Correspondence to:* Fanghua Xu ([fxu@mail.tsinghua.edu.cn](mailto:fxu@mail.tsinghua.edu.cn))

8

9 **Abstract.** Sea spray-mediated heat flux plays an important role in air-sea heat transfer. Heat flux  
10 integrated over droplet size spectrum can well simulate total heat flux induced by sea spray droplets.  
11 Previously, a fast algorithm of spray-flux assuming single-radius droplets (A15) was widely used since  
12 the full-size spectrum integral is computationally expensive. Based on the Gaussian Quadrature (GQ)  
13 method, a new fast algorithm (SPRAY-GQ) of sea spray-mediated heat flux is derived. The performance  
14 of SPRAY-GQ is evaluated by comparing heat fluxes with those estimated from the widely-used A15.  
15 The new algorithm shows a better agreement with the original spectrum integral. To further evaluate the  
16 numerical errors of A15 and SPRAY-GQ, the two algorithms are implemented into a coupled CFSv2.0-  
17 WW3 system, and a series of 56-day simulations in summer and winter are conducted and compared.  
18 The comparisons with satellite measurements and reanalysis data show that the SPRAY-GQ algorithm  
19 could lead to more reasonable simulation than the A15 algorithm by modifying air-sea heat flux. For  
20 experiments based on SPRAY-GQ, the sea surface temperature at mid-high latitudes of both hemispheres,  
21 particularly in summer, is significantly improved compared with the experiments based on A15. The  
22 simulation of 10-m wind speed and significant wave height at mid-low latitudes of the Northern  
23 Hemisphere after the first two weeks is improved as well. The computational time of SPRAY-GQ is  
24 about the same as that of A15. Thereby, the newly-developed SPRAY-GQ algorithm has a potential to  
25 be used for calculation of spray-mediated heat flux in coupled models.

26

## 27 **1 Introduction**

28 Sea spray droplets, ejected from oceans, include film drops, jet drops and spume drops (Veron, 2015).  
29 The first two types of droplets are generated from bubble bursting caused by ocean surface wave breaking,  
30 with radius ranging from 0.5  $\mu\text{m}$  to 50  $\mu\text{m}$  (Resch and Afeti, 1991; Thorpe, 1992; Melville, 1996; Spiel,  
31 1997; Andreas, 1998; Lhuissier and Villermaux, 2012). Spume drops are generated by strong winds ( $>$   
32 7-11 m/s) which directly tear the wave crests, with larger radius ranging from tens to hundreds of  
33 micrometers (Koga, 1981; Andreas et al., 1995; Andreas, 1998). Sea spray droplets play an important  
34 role in weather and climate processes (Fox-Kemper et al., 2022). On one hand, sea spray droplets  
35 contribute to local marine aerosols and subsequently modify the local radiation balance (Fairall et al.,  
36 1983; Burk, 1984; Fairall and Larsen, 1984). On the other hand, sea spray droplets affect the fluxes of  
37 heat, momentum, salt, and freshwater between atmosphere and ocean (Andreas, 1992; Andreas et al.,  
38 2008; Andreas, 2010; Andreas et al., 2015; Ling and Kao, 1976; Fairall et al., 1994; Andreas and  
39 Decosmo, 2002).

40 The sea spray-mediated heat transfer mainly occurs within the droplet evaporation layer (DEL) near  
41 the sea surface (Andreas and Decosmo, 1999, 2002; Fairall et al., 1994). Sea spray droplets with the same  
42 temperature as ocean surface can lead to sensible heat flux in DEL, while water evaporated from these  
43 droplets can further release latent heat to the atmosphere (Andreas, 1992; Borisenkov, 1974; Bortkovskii,  
44 1973; Wu, 1974; Monahan and Van Patten, 1988; Ling and Kao, 1976). Part of the sea spray-mediated  
45 sensible heat is absorbed by droplet evaporation, which further increases the air-sea temperature  
46 difference, and thus increases the sea spray-mediated sensible heat flux (Fairall et al., 1994; Andreas and  
47 Decosmo, 2002). Since strong winds produce more sea spray droplets with larger radius, sea spray-  
48 mediated heat fluxes increase with wind speed (Fairall et al., 1994), and contribute more than 10% of the  
49 total surface heat flux after reaching the threshold speed ( $>$  11 m/s for sensible heat flux and  $>$  13 m/s  
50 for latent heat flux)(Andreas et al., 2008). In addition, when a droplet is released into the air, it is  
51 accelerated due to surface winds (Edson and Andreas, 1997; Fairall et al., 1994; Van Eijk et al., 2011;  
52 Wu et al., 2017). If the droplet could fall back into the ocean, additional momentum would be injected  
53 into the ocean from the atmosphere (Andreas, 1992, 2004).

54 The usual bulk parameterizations in numerical models for surface fluxes only include the interfacial

55 (turbulent) fluxes (e.g., Fairall et al., 1996), while neglecting the significant contributions of sea spray  
56 droplets in DEL (Andreas et al., 2008; Fairall et al., 1994; Smith, 1997; Emanuel, 1995). Andreas and  
57 Emanuel (2001) implemented sea spray-mediated heat flux and momentum flux parameterizations into  
58 a simple tropical cyclone model, and found that the sea spray-mediated heat flux can significantly  
59 enhance tropical cyclone intensity. It is well known that strong winds and high waves induced by tropical  
60 cyclones can enhance sea surface roughness and thus surface drag coefficients, which tend to reduce  
61 tropical cyclone intensity (Emanuel, 1995). Furthermore, the accelerated sea spray droplets by surface  
62 winds also lead to more dissipation of tropical cyclone kinetic energy (Andreas, 1992, 2004). These  
63 negative effects could be offset by the sea spray-mediated heat flux. The similar enhancement of tropical  
64 cyclone intensity was also noticed in recent regional coupling systems by including sea spray-mediated  
65 heat flux (Xu et al., 2021b; Liu et al., 2012; Garg et al., 2018; Zhao et al., 2017). In the First Institute of  
66 Oceanography Earth System Model, Bao et al. (2020) first incorporated the sea spray-mediated heat flux  
67 in global climate simulation. Following Bao et al. (2020), Song et al. (2022) found that the sea spray-  
68 mediated heat flux can lead to cooling at the air-sea interface and strengthening westerlies in the Southern  
69 Ocean, and thus improves estimates of sea surface temperature (SST).

70 Since the parameterization of sea spray-mediated heat flux derived from observations requires full-  
71 size spectral integral and thus computationally expensive for large-scale models (Table 1, details in  
72 Section 4.2; Andreas, 1989, 1990, 1992; Andreas et al., 2015), a simplified algorithm based on a single  
73 radius of sea spray droplets (Andreas et al., 2015; Andreas et al., 2008) is widely used in atmosphere-  
74 ocean coupling systems (Xu et al., 2021b; Liu et al., 2012; Garg et al., 2018; Zhao et al., 2017; Song et  
75 al., 2022; Bao et al., 2020), and apt to produce numerical errors. To reduce these numerical errors induced  
76 by the single radius of sea spray droplets, we develop a new fast algorithm of sea spray-mediated heat  
77 flux based on the Gaussian Quadrature (GQ) method, a fast and accurate way to calculate spectral integral.  
78 The GQ method has been successfully used for the estimation of domain-averaged radiative flux profiles  
79 (Li and Barker, 2018). The performance of the GQ-based fast algorithm of the sea spray-mediated heat  
80 flux is evaluated and compared with the simplified algorithm for single radius of Andreas et al. (2015),  
81 referred to as A15 hereafter. The results are first compared with the original parameterization using full-  
82 size spectral integral (A92, hereafter). Then the parameterizations with different algorithms are

83 implemented in a global coupled atmosphere-ocean-wave system (Shi et al., 2022), and the results are  
84 compared with global satellite measurements and reanalysis data.

85 The rest of the paper is structured as follows: observation and reanalysis data for comparisons are  
86 introduced in Section 2; the derivation of the GQ-based fast algorithm and the global coupling system  
87 are described in Section 3; the performance of the new fast algorithm is evaluated in Section 4. Finally,  
88 a summary and discussion are given in Section 5.

## 89 **2 Data**

90 The fifth generation European Centre for Medium-Range Weather Forecasts (ECMWF) Reanalysis  
91 (ERA5; Hersbach et al., 2020) 10-m wind speed (WSP10), 2-m air temperature (T02), 2-m dewpoint  
92 temperature, surface pressure and significant wave height (SWH) with a spatial resolution of  $0.5^\circ$  are  
93 used. Additionally, WSP10, T02 and 2-m specific humidity (SPH) data from the Objectively Analyzed  
94 air-sea Fluxes (OAFlux) products (Yu et al., 2008) are also applied for comparison, with  $1^\circ \times 1^\circ$  resolution.  
95 The daily average satellite Optimum Interpolation SST (OISST) data are obtained from the National  
96 Oceanic and Atmospheric Administration (NOAA) with a spatial resolution of  $0.25^\circ$  (Reynolds et al.,  
97 2007). The global monthly mean salinity observations from European Space Agency (ESA;  
98 [https://climate.esa.int/sites/default/files/SSS\\_cci-D1.1-URD-v1r4\\_signed-accepted.pdf](https://climate.esa.int/sites/default/files/SSS_cci-D1.1-URD-v1r4_signed-accepted.pdf)) are applied.  
99 Besides, we also use the monthly global ocean RSS Satellite Data Products for WSP10  
100 ([https://data.remss.com/wind/monthly\\_1deg/](https://data.remss.com/wind/monthly_1deg/)) and the Reprocessed L4 Satellite Measurements for SWH  
101 (<https://doi.org/10.48670/moi-00177>), to validate the simulation results and ERA5 data.

## 102 **3 Methods**

### 103 **3.1 Development of a Fast Algorithm Based on GQ**

104 The effects of sea spray droplets on sensible and latent heat fluxes ( $H_{S,SP}$ ,  $H_{L,SP}$ ) contribute to the total  
105 turbulent sensible and latent heat fluxes ( $H_{S,T}$ ,  $H_{L,T}$ ) at the air-sea interface. That is,

$$H_{S,T} = H_S + H_{S,SP}, \quad (1)$$

$$H_{L,T} = H_L + H_{L,SP}. \quad (2)$$

106 where  $H_S$  and  $H_L$  are the sensible and latent heat fluxes at the air-sea interface due to the air-sea  
 107 differences of temperature and humidity. Based on observations of total turbulent heat fluxes and the  
 108 COARE algorithm (Andreas et al., 2015; Fairall et al., 1996), A92 integrates the sea spray-mediated  
 109 sensible and latent heat flux spectrums over initial droplet radius ( $Q_S(r_0)$  and  $Q_L(r_0)$ ) to estimate  $H_{S,SP}$   
 110 and  $H_{L,SP}$  (details in Appendix A; Andreas, 1989, 1990, 1992; Andreas and Decosmo, 2002). The  
 111 distributions of  $Q_S(r_0)$  and  $Q_L(r_0)$  spectrums as functions of initial droplet radius  $r_0$  under various  
 112 atmosphere and ocean state are shown in Fig. 1, indicating that  $Q_S$  and  $Q_L$  spectrums are more  
 113 sensitive to the change of WSP10, and less sensitive to other variables, including T02, 2-m relative  
 114 humidity, SST, surface air pressure and sea surface salinity.

115 The calculation of  $H_{S,SP}$  and  $H_{L,SP}$  in A92 is computationally expensive due to full-size spectral  
 116 integral (Eqn. A5-A6 of Appendix A), therefore it is difficult to apply A92 directly in coupled modeling  
 117 systems. A15 (Andreas et al., 2015) developed a fast algorithm by using a single representative droplet  
 118 radius (details in Appendix B), which was widely adopted in recent regional and global coupling systems  
 119 (Xu et al., 2021b; Liu et al., 2012; Garg et al., 2018; Zhao et al., 2017; Song et al., 2022; Bao et al., 2020).  
 120 In this study, we apply a 3-node GQ method (details in Appendix C) to develop a new fast algorithm to  
 121 approximate the full-size spectral integral of A92. Notably, GQ can converge exponentially to the actual  
 122 integral only for a smooth function, which is a prerequisite for GQ (McClarren, 2018). Since as functions  
 123 of  $r_0$ ,  $Q_S(r_0)$  and  $Q_L(r_0)$  are not smooth (Fig. 1), a data sorting from largest to smallest is required.  
 124 After sorting, local  $Q_S(r_0)$  and  $Q_L(r_0)$  become  $Q_{S\_sort}(m)$  and  $Q_{L\_sort}(m)$ , and then GQ can be used  
 125 to estimate the integral of  $Q_{S\_sort}(m)$  and  $Q_{L\_sort}(m)$ . Note that the independent variable  $m$  is not  
 126 equivalent to the original  $r_0$ , but only indicates the position. In this way, according to Appendix C,  
 127  $m_1=443$ ,  $m_2=251$ ,  $m_3=58$  are three GQ nodes of  $Q_{S\_sort}(m)$  and  $Q_{L\_sort}(m)$ , and we can get the  
 128 corresponding  $r_0$  for local  $Q_S$  ( $Q_L$ ), denoted as  $r_{S1}(r_{L1})$ ,  $r_{S2}(r_{L2})$  and  $r_{S3}(r_{L3})$ . However, the  
 129 sorting leads to high complexity of GQ comparable to A92, and the values of  $r_{S1}(r_{L1})$ ,  $r_{S2}(r_{L2})$  and  
 130  $r_{S3}(r_{L3})$  vary under various atmosphere and ocean environments in the globe. Therefore, it is necessary  
 131 to find the general approximate values of  $r_{S1}(r_{L1})$ ,  $r_{S2}(r_{L2})$  and  $r_{S3}(r_{L3})$  via global statistical  
 132 analyses, to avoid the sorting in application.

133 To derive the general approximate values of  $r_{S1}(r_{L1})$ ,  $r_{S2}(r_{L2})$  and  $r_{S3}(r_{L3})$ , we calculate the

134 distribution of the sea spray-mediated heat flux spectral following A92, based on the global daily WSP10,  
 135 T02, 2-m dewpoint temperature, surface pressure and SWH of ERA5 and OISST from August 1, 2018  
 136 to August 31, 2018. Since the sea spray-mediated heat flux is not sensitive to salinity (Fig. 1e&f) and  
 137 only monthly observational data is available, the ESA monthly salinity is applied. From the global  
 138 spectrums, we sort  $Q_S$  and  $Q_L$  from largest to smallest to obtain local  $r_{S1}$ ,  $r_{S2}$  and  $r_{S3}$  ( $r_{L1}$ ,  $r_{L2}$  and  
 139  $r_{L3}$ ) for every grid point, whose global distribution of occurrence frequency in percentage is shown in  
 140 Fig. 2. It is noted that except for  $r_{L3}$ , all other five nodes have frequency roughly concentrated at a  
 141 constant (peak frequency >65% in Fig. 2a, b, d-f; Eqn. 3&4), while for  $r_{L3}$ , there is a 92.53%  
 142 concentration between 55 and 90  $\mu m$  (Fig. 2c). Then we found that  $r_{L3}$  (55-90  $\mu m$ ) is related to WSP10  
 143 (Fig. S1 in supplementary), thereby we set the approximate values as

$$r_{S1} = 459.056, r_{S2} = 294.185, r_{S3} = 166.771, \quad (3)$$

$$r_{L1} = 443.914, r_{L2} = 251.0498, \quad (4)$$

$$r_{L3} = \begin{cases} 60.310WSP10^{0.1161}, & WSP10 \geq 2 \text{ m/s} \\ 58.086, & WSP10 < 2 \text{ m/s} \end{cases}, \quad (5)$$

144 where the unit of the radius is micrometer. Afterwards, we directly use Eqn. 3-5 to approximate the full-  
 145 size spectral integral of A92 without sorting as

$$\int_a^b Q_S(r_0) dr_0 \approx \frac{b-a}{2} \sum_{i=1}^3 \omega_i Q_S(r_{Si}), \quad (6)$$

$$\int_a^b Q_L(r_0) dr_0 \approx \frac{b-a}{2} \sum_{i=1}^3 \omega_i Q_L(r_{Li}). \quad (7)$$

146 Here a and b are the lower and upper limits of  $r_0$ , which are set to  $2\mu m$  and  $500\mu m$  based on Andreas  
 147 (1990), and  $\omega_i$  is the corresponding weight ( $\omega_1=\omega_3=0.556$ ,  $\omega_2=0.889$ ), obtained from Mcclarren  
 148 (2018). The new fast algorithm for approximations of  $H_{S,SP}$  and  $H_{L,SP}$  is referred to as SPRAY-GQ  
 149 hereafter.

### 150 3.2 CFSv2.0-WW3 Coupling System

151 A coupled system based on Climate Forecast System model version 2.0 (CFSv2.0) and  
 152 WAVEWATCH III (WW3) is employed to evaluate and compare the effects of sea spray-mediated heat  
 153 flux parameterized by A15 and SPRAY-GQ. The CFSv2.0-WW3 has three components, the Global

154 Forecast System (GFS; <http://www.emc.ncep.noaa.gov/GFS/doc.php>) as the atmosphere component of  
155 CFSv2.0, the Modular Ocean Model version 4 (MOM4; Griffies et al., 2004) as the ocean component of  
156 CFSv2.0, and the WW3 (WAVEWATCH III Development Group, 2016) as the ocean surface wave  
157 component. The variables between CFSv2.0 and WW3 are interpolated and passed using the Chinese  
158 Community Coupler version 2.0 (C-Coupler2; Liu et al., 2018).

159 The CFSv2.0 is mainly applied for intraseasonal and seasonal prediction (e.g., Saha et al., 2014). The  
160 atmosphere component GFS uses a spectral triangular truncation of 382 waves (T382) in the horizontal,  
161 equivalent to a grid resolution of nearly 35 km, and 64 sigma-pressure hybrid layers in the vertical. The  
162 MOM4 is integrated on a nominal 0.5° horizontal grid with enhanced horizontal resolution to 0.25° in  
163 the tropics, and there are 40 levels in the vertical. The CFSv2.0 initial fields at 00:00 UTC of the first  
164 day for experiments were generated by the real time operational Climate Data Assimilation System  
165 (Kalnay et al., 1996), downloaded from the CFSv2.0 official website  
166 (<http://nomads.ncep.noaa.gov/pub/data/nccf/com/cfs/prod>). The latitude range of WW3 is 78°S–78°N  
167 with a spatial resolution of 1/3°. The initial wave fields were generated from 10-day simulation starting  
168 from rest in a stand-alone WW3 model, forced by ERA5 10-m winds and ice concentration. The open  
169 boundary conditions of WW3 were also obtained by the global simulation of the stand-alone WW3 model.

170 In the coupling system, the WW3 obtains 10-m wind and ocean surface current from CFSv2.0, and  
171 then provides wave parameters to CFSv2.0. Several wave-mediated processes, including upper ocean  
172 mixing modified by Stokes drift-related processes, air-sea fluxes modified by surface current and Stokes  
173 drift, and momentum roughness length, are considered. Details of this system are referred to Shi et al.  
174 (2022).

175 A series of numerical experiments is conducted to evaluate the effects of the two fast algorithms (A15  
176 and SPRAY-GQ) of sea spray-mediated heat flux on ocean, atmosphere and waves in two 56-day periods,  
177 from January 3 to February 28, 2017 and from August 3 to September 28, 2018 for boreal winter and  
178 boreal summer, respectively. For each period, two sensitivity experiments are carried out. The first is the  
179 SPRAY-A15 experiment, in which A15 is used with two-way fully coupling. The second is the SPRAY-  
180 GQ experiment, in which SPRAY-GQ fast algorithm is used instead of A15. In addition, we also carry  
181 out another 7-day experiment using A92 (SPRAY-A92) to test the runtime.



## 182 4 Results

### 183 4.1 Comparison with A92

184 Based on the daily global WSP10, T02, 2-m dewpoint temperature, surface pressure and SWH of  
185 ERA5, the daily global OISST, and the ESA monthly global salinity,  $H_{S,SP}$  and  $H_{L,SP}$  from A15,  
186 SPRAY-GQ and A92 are calculated (Fig. 3). The computational time for SPRAY-GQ is about the same  
187 as that for A15, and about 36 times less than the time for A92. Compared with A92 (the black dotted  
188 line), A15 (red) overestimates  $H_{S,SP}$  for low  $H_{S,SP}$  ( $<50$  W/m<sup>2</sup>) and underestimates  $H_{S,SP}$  for high  
189  $H_{S,SP}$  ( $>50$  W/m<sup>2</sup>) with a root mean square error (RMSE= $\sqrt{\sum_{i=1}^n(\hat{y}_i - y_i)^2/n}$ ,  $\hat{y}_i$  is A15 value,  $y_i$  is  
190 A92 value, and  $n$  is the total number of grid points) of 3.40 W/m<sup>2</sup> (Fig. 3a), while A15 shows consistent  
191 overestimations with a RMSE of 2.98 W/m<sup>2</sup> for  $H_{L,SP}$  (Fig. 3b). Overall, the RMSE of A15 is about  
192 2.69 W/m<sup>2</sup> for sea-spray mediated total heat flux ( $TH_{SP} = H_{S,SP} + H_{L,SP}$ ; Fig. 3c). Andreas et al. (2015)  
193 derived A15 from A92 using single-radius droplets as bellwethers and wind functions, and extrapolated  
194 the wind functions at high wind speeds  $>25$  m/s. Since the wind speeds in the study are less than 25 m/s  
195 (Fig. S1), the large difference between A15 and A92 is mainly due to the use of single-radius droplets.  
196 Compared with A15, SPRAY-GQ (blue) has less deviation from A92 for both  $H_{S,SP}$  and  $H_{L,SP}$  (Fig.  
197 3a&b). The corresponding RMSEs of SPRAY-GQ for  $H_{S,SP}$ ,  $H_{L,SP}$  and  $TH_{SP}$  are 0.83 W/m<sup>2</sup>, 0.92  
198 W/m<sup>2</sup> and 0.62 W/m<sup>2</sup>, all significantly lower ( $P<0.05$  in Student's t-test) than those of A15.

199 To test robustness of the results, we also use WSP10, T02 and SPH of OAFlux dataset to estimate  
200  $H_{S,SP}$  and  $H_{L,SP}$ . As shown in Fig. 4, SPRAY-GQ has significantly ( $P<0.05$  in Student's t-test) lower  
201 deviations and RMSEs than A15, consistent with Fig. 3. Note that the values of  $H_{S,SP}$  and  $H_{L,SP}$  in  
202 Fig.4 are larger than those in Fig. 3. It is because OAFlux only provides neutral wind speeds, calculated  
203 from wind stress and the corresponding roughness by assuming air is neutrally stratified. The neutral  
204 winds from OAFlux are larger than winds in ERA5 as indicated by previous studies (Lindemann et al.,  
205 2021; Seethala et al., 2021).

206 In addition, since it is common to derive SWH from empirical equations (e.g., Andreas et al., 2008;  
207 Andreas et al., 2015; Andreas and Decosmo, 2002; Andreas, 1992), we also use SWH generated by  
208 empirical equations of WSP10 (Andreas, 1992) instead of ERA5 SWH to estimate  $H_{S,SP}$  and  $H_{L,SP}$

209 (Fig. 5). Again, the RMSEs decrease significantly ( $P < 0.05$  in Student's t-test) in SPRAY-GQ compared  
210 to A15, though the RMSEs become higher for all estimates due to the enhanced biases of SWH. The  
211 difference between SPRAY-GQ and A92 is always smaller than that between A15 and A92. Next, we  
212 will evaluate and compare the two fast algorithms in an atmosphere-ocean-wave coupled system  
213 (CFSv2.0-WW3).

## 214 **4.2 Comparison in the CFSv2.0-WW3 Coupling System**

215 To compare the computational time of different parameterizations in the large-scale modeling system,  
216 the runtime of the fully coupled experiments for 7-day forecast is given in Table 1 as an example. It is  
217 shown that the runtime is about the same for SPRAY-GQ and SPRAY-A15. Both experiments run about  
218 17 times faster than SPRAY-A92.

219 To illustrate the numerical errors of the two fast algorithms discussed in the context of the coupled  
220 system, comparisons are made for simulated SSTs, WSP10s as well as SWHs against OISST and ERA5  
221 reanalysis. The results in the first three days are excluded in the comparison, since the wave influences  
222 are weak at the beginning of the simulations. Overall, the WSP10s of simulations are generally in the  
223 range of 0-25 m/s globally. At mid-high latitudes, the WSP10s generally exceed 10 m/s (Fig. S2&S3 of  
224 the supplementary), at which the effects of sea spray can become significant (Andreas et al., 2015;  
225 Andreas et al., 2008).

### 226 **4.2.1 Sea Surface Temperature (SST)**

227 In the austral summer, compared with OISST, large SST biases ( $>1$  °C or  $<-1$  °C) of SPRAY-A15  
228 occur in the Southern Hemisphere (SH; Fig. S4a in supplementary), especially in the Southern Ocean. It  
229 is always a challenge for reducing the large SST biases in the Southern Ocean for climate models (e.g.,  
230 Alessandro et al., 2019; Wang et al., 2014; Li et al., 2013; Bodas-Salcedo et al., 2012; Ceppi et al., 2012).  
231 In Fig. 6a, SSTs north (south) of 50°S in experiment SPRAY-A15 are mainly underestimated  
232 (overestimated). The domain-averaged RMSE (0-360°E, 40-75°S) increases in the first month and then  
233 levels off (red solid line in Fig. 6c). While the domain-averaged RMSE in experiment SPRAY-GQ levels  
234 off about a week earlier (black solid line in Fig. 6c). The mean RMSE in SPRAY-GQ is significantly

235 lower than that in SPRAY-A15 ( $P < 0.05$  in Student's t-test). The increased (decreased) SSTs north (south)  
 236 of 50°S in SPRAY-GQ compared to those in SPRAY-A15 (Fig. 6b) reduce the RMSE of SST in SPRAY-  
 237 GQ. We also calculate the mean absolute error,  $MAE = \sum_{i=1}^n |\hat{y}_i - y_i|/n$ , where  $\hat{y}_i$  is simulated value  
 238 and  $y_i$  is OISST data, and  $n$  is the total number of grid points. The MAEs are consistent with RMSEs  
 239 (dotted line in Fig. 6c). Furthermore, the mean errors,  $ME = \sum_{i=1}^n (\hat{y}_i - y_i)/n$  (Fig. S5a in the  
 240 supplementary), are smaller in SPRAY-GQ than SPRAY-A15.

241 To understand the effects of sea spray droplets on SST, we calculate the total heat flux ( $TH = H_{S,T} + H_{L,T}$ )  
 242 differences between SPRAY-GQ and SPRAY-A15 (Fig. 7a). The TH differences are significantly  
 243 correlated with SST differences (Fig. S4b in the supplementary), with the spatial correlation coefficient  
 244 of -0.41 ( $P < 0.05$  in Student's t-test). We further decompose direct and indirect effects of sea spray  
 245 droplets on heat fluxes following Song et al. (2022). The direct effect ( $H_{S,SP}$  and  $H_{L,SP}$ ) is induced  
 246 directly by sea spray droplets, calculated from A15 (Eqn. B1-B4 of Appendix B) and SPRAY-GQ  
 247 (Section 3.1). The indirect effect ( $H_S$  and  $H_L$ ) is the heat flux variation induced by changes of  
 248 atmosphere and ocean variables (including wind, pressure, humidity and temperature) caused by direct  
 249 effect, estimated by subtracting  $H_{S,SP}$  and  $H_{L,SP}$  from the output heat fluxes ( $H_{S,T}$  and  $H_{L,T}$ ) of  
 250 experiment SPRAY-A15 and SPRAY-GQ.

251 In the Southern Ocean, although direct differences of  $H_{S,SP}$  and  $H_{L,SP}$  are relatively small ( $< 10$   
 252  $W/m^2$ , Fig. 7b, e, & h), the resulting changes of temperature and humidity lead to relatively large  
 253 differences in indirect effects of  $H_S$  and  $H_L$  (Fig. 7c, f, & i). Enhanced (reduced)  $TH_{SP}$  from ocean to  
 254 atmosphere in the summer leads to increased (decreased) air-sea temperature difference and thus  
 255 enhances (weakens)  $H_S$ . Meanwhile the warmer (cooler) air also causes more (less) evaporation and thus  
 256 more (less)  $H_L$ . Finally, the enhanced (reduced) TH cools (warms) SST.

257 In the boreal summer, large SST biases ( $> 1$  °C or  $< -1$  °C) of SPRAY-A15 mainly occur at mid-high  
 258 latitudes of the Northern Hemisphere (NH; Fig. S6a in supplementary). Significant underestimations  
 259 occur in the western and northern part of the North Pacific and at mid latitudes of the North Atlantic,  
 260 while large positive SST biases mainly occur in the eastern part of the North Pacific and at high latitudes  
 261 of the North Atlantic (Fig. 8a). In experiment SPRAY-GQ, SSTs are warmer (cooler) in the previously  
 262 underestimated (overestimated) regions (Fig. 8b). Therefore, the domain-averaged RMSE and MAE (0-

263 360°E, 20-75°N) in SPRAY-GQ are significantly lower ( $P < 0.01$  in Student's t-test) than in SPRAY-A15  
264 after the first three weeks (Fig. 8c). Compared to SPRAY-A15, the overall underestimation is reduced in  
265 SPRAY-GQ (Fig. S5b). The spatial correlation coefficient between TH differences and SST differences  
266 (Fig. 9a&Fig. S6b) is -0.32 ( $P < 0.05$  in Student's t-test). Consistent with the austral summer, the SST  
267 changes are related to the changes of heat flux (Fig. 9). The indirect effects of latent heat flux (Fig. 9f)  
268 play a major role in TH differences, which are modified by the direct effects (Fig. 9b, e, &h). In addition,  
269 the changes of surface wind also contribute to the changes of SST. The reduced winds weaken the upper  
270 ocean mixing, the water becomes more stratified, and then the SST tends to be warmer, and vice versa  
271 (Fig. S7&S8).

#### 272 **4.2.2 10-m Wind Speed (WSP10) and Significant Wave Height (SWH)**

273 Compared with experiment SPRAY-A15, significant differences of WSP10 in SPRAY-GQ occur at  
274 mid-low latitudes of the NH (0-360°E, 0-60°N) in both winter and summer (Fig.S7b&S8b). As we know,  
275 satellite scatterometer and altimeter data are usually used to validate WSP10 and SWH for short term  
276 weather forecast (e.g., Accadia et al., 2007; Djurdjevic and Rajkovic, 2008; Myslenkov et al., 2021).  
277 However, due to the spatial and temporal coverage of satellite data, we can only obtain the monthly  
278 averaged satellite data for the globe. So we compare the monthly averaged WSP10 and SWH from  
279 simulations with the corresponding satellite data (Fig. S9-S12). The comparison results (Fig. S9a&c-  
280 S12a&c) are consistent with those compared with ERA5 (Fig. S9b&d-S12b&d). From Fig. S9e-S12e,  
281 the differences of WSP10s between ERA5 and the satellite data are always less than 1 m/s and the  
282 differences of SWHs are always less than 0.3 m. Since ERA5 provides daily data for comparison, we  
283 will use ERA5 for validation in the following.

284 The ME of WSP10 (SPRAY-A15 minus ERA5) is 0.28 m/s and 0.47 m/s in winter and summer (red  
285 in Fig. S5c&d), respectively, mainly due to the overestimations over the Pacific and the Atlantic Ocean  
286 (red in Fig.10a&11a). Whereas in SPRAY-GQ, the ME (SPRAY-GQ minus ERA5) is 0.15 m/s and 0.33  
287 m/s in winter and summer respectively (black in Fig. S5c&d). The domain-averaged RMSEs and MAEs  
288 of WSP10s increase with time in the first two weeks and then gradually level off (Fig. 10c&11c). The  
289 differences of WSP10 RMSEs and MAEs between SPRAY-GQ (black) and SPRAY-A15 (red) are very

290 small in the first two weeks. Afterwards the mean values of RMSE and MAE in SPRAY-GQ are lower  
291 than those in SPRAY-A15 significantly at 95% confidence level in both boreal winter (Fig. 10c) and  
292 boreal summer (Fig. 11c).

293 The simulated SWHs changes are closely related to the changes of WSP10s (Shi et al., 2022).  
294 Therefore, the differences of SWHs (Fig.12&13) are consistent with those of WSP10s (Fig.10&11), with  
295 overestimated (underestimated) WSP10s corresponding to overestimated (underestimated) SWHs  
296 compared with ERA5. The SWHs in SPRAY-GQ are significantly different with those in SPRAY-A15  
297 (Fig. 12b&13b). In winter (summer), the SWH RMSE averages for SPRAY-A15 and SPRAY-GQ are  
298 1.31 m (0.98 m) and 1.23 m (0.87 m), and after the first two weeks the RMSE and MAE in SPRAY-GQ  
299 are lower than those in SPRAY-A15 significantly at 95% confidence level in both winter (Fig. 12c) and  
300 summer (Fig. 13c).

301 The direct and indirect effects of sea spray droplets on heat fluxes can influence estimates of WSP10  
302 and then SWH. The changes of WSP10s are related to the direct effects ( $H_{S,SP}$  and  $H_{L,SP}$ ; Fig. 7b, e, &h;  
303 Fig. 9b, e, &h). The spatial correlation coefficients between WSP10 differences (Fig. S7b&S8b) and  
304  $TH_{SP}$  differences (Fig. 7b&9b) are 0.51 and 0.69 ( $P < 0.01$  in Student's t-test) in winter and summer,  
305 respectively. Because  $TH_{SP}$  differences can influence the sea level pressure (SLP) distribution (Fig.  
306 S15&S16), and subsequently surface winds. For example, compared with SPRAY-A15, the decreased  
307  $TH_{SP}$  of SPRAY-GQ in the Northwest Pacific in summer (Fig. 9b) leads to higher SLP and smaller  
308 pressure gradient (Fig. S16), and thus decreased WSP10 (Fig. 11b); while the increased  $TH_{SP}$  in the  
309 Gulf of Alaska (Fig. 9b) leads to lower SLP and larger pressure gradient (Fig. S16), and thus enhanced  
310 WSP10 (Fig. 11b). The accelerated (decelerated) WSP10s further result in increased (decreased)  
311 interfacial heat transport ( $H_S$ ,  $H_L$ ), as well as increased (decreased) SWHs.

## 312 **5 Conclusions and Discussion**

313 Based on a GQ method, we develop a new fast algorithm based on Andreas's (1989, 1990, 1992) full-  
314 size microphysical parameterization (A92) for sea spray-mediated heat fluxes. Using global satellite  
315 measurements and reanalysis data, we found that the difference between SPRAY-GQ and A92 is  
316 significantly smaller than that between A15 and A92 (Andreas et al., 2015). To evaluate the numerical

317 error of SPRAY-GQ/A15 fast algorithm, we implement them in the two-way coupled CFSv2.0-WW3  
318 system. A series of 56-day simulations from January 3 to February 28, 2017 and from August 3 to  
319 September 28, 2018 are conducted. The results are compared against satellite measurements and ERA5  
320 reanalysis. The comparison shows that the sea spray-mediated heat flux in SPRAY-GQ can reasonably  
321 modulate total heat flux compared with SPRAY-A15, and significantly reduce the SST biases in the  
322 Southern Ocean (mid-high latitudes of the NH) for the austral (boreal) summer, as well as WSP10 and  
323 SWH after the first two weeks at mid-low latitudes of the NH for both boreal winter and summer. Overall,  
324 our fast algorithm based on GQ is applicable to sea spray-mediated heat flux parameterization in coupled  
325 models.

326 To investigate the effects of spray-mediated heat flux on simulations, two 56-day experiments without  
327 sea spray effect (CTRL) in boreal winter and summer respectively are conducted, and the differences of  
328 simulated SST, WSP10, SWH, T02 and SPH between SPRAY-GQ and CTRL are compared in Fig. S17-  
329 S21 in the supplementary. The introduction of sea spray cannot significantly reduce the global overall  
330 errors of simulations, but it leads to regional improvements (blue in Fig. S17e&f-S21e&f). For example,  
331 compared with CTRL in Jan-Feb, 2017, SST MAE of SPRAY-GQ in the southeast of Australia decreases  
332 (Fig. S17e), because of warmer SST (Fig. S17c) related to reduced wind (Fig. S18c). The reduced wind  
333 here also leads to lower SWH (Fig. S19c) and thus reduced SWH overestimation (Fig. S19e). Meanwhile,  
334 SPRAY-GQ reduces MAE of T02 and SPH (Fig. S20e&S21e) by increasing temperature and moisture  
335 (Fig. S20c&S21c). The reduced errors are related to the relatively large WSP10s over the areas (Fig.  
336 S2&S3), since the effects of sea spray become important at wind speeds larger than 10 m/s.

337 In addition to the variables aforementioned, the changes of simulated cloud fraction were also  
338 compared. However, the effects of sea spray-mediated heat flux on cloud fraction are non-significant for  
339 the 2-month simulation, so the results are not shown. Besides, the lack of other processes related to sea  
340 spray may be one of reasons why the global overall error cannot be reduced effectively. For example, for  
341 simulated WSP10 and SWH in SPRAY-GQ, the significant overestimations in the SH still exist  
342 especially in Aug-Sep, 2018 (Fig. S18&S19 in supplementary). As Andreas (2004) indicated, sea spray  
343 droplets also influence the surface momentum flux by injecting more momentum into the ocean from the  
344 atmosphere, which might further decrease the surface wind speed. We will consider this process in the

345 future study.

346 Sea spray-mediated heat fluxes are related to the sea spray generation function (SSGF). Based on a  
347 number of laboratory and field observations, varieties of SSGF were derived (e.g., Koga, 1981; Monahan  
348 et al., 1982; Troitskaya et al., 2018; Andreas, 1992, 1998, 2002; Fairall et al., 1994; Veron, 2015),  
349 whereas their differences can reach six orders of magnitude (Andreas, 1998). There is currently no  
350 consensus on the most suitable choice. In this study, we use SSGF of Fairall et al. (1994), recommended  
351 by Andreas (2002), to get a mean bias of 3.70 W/m<sup>2</sup> and 0.095 W/m<sup>2</sup> for latent and sensible heat flux  
352 respectively (Andreas et al., 2015), consistent with recent observations of Xu et al. (2021a). Even though,  
353 the improved SST and other variables cannot be reliably assigned to the usage of the GQ method, due to  
354 the uncertainties of the coupled model itself and SSGF.

355 When wind speed is larger than 10 m/s, spray-mediated heat flux can become as important as the  
356 interfacial heat flux (Andreas and Decosmo, 1999, 2002). Particularly, even in the absence of air-sea  
357 temperature difference, the spray-mediated sensible heat flux is still present (Andreas et al., 2008). As  
358 indicated by previous studies (e.g., Garg et al., 2018; Song et al. 2022), it is necessary to superimpose  
359 the spray-mediated heat flux on the bulk formula to complete the physics of turbulent heat transfer for  
360 coupled simulation. Since the full microphysical parameterization (A92) is computationally expensive,  
361 an efficient algorithm that captures the main features of A92 can be beneficial to large-scale climate  
362 systems or operational storm models. The GQ method proposed in the study can efficiently calculate the  
363 spray-mediated heat flux, and agree better with A92 than A15. Thereby, the GQ based spray-mediated  
364 heat flux is promising to be widely applied in large-scale climate systems and operational storm models.

365

## 366 **Appendix A**

### 367 **Microphysical Parameterization of A92**

368 Based on the cloud microphysical parameterization of Pruppacher and Klett (1978), Andreas (1989,  
369 1990, 1992) proposed a parameterization of sea spray-related heat fluxes for droplets with different radius,  
370 from formation at sea surface to equilibrium with environment, that is,

$$Q_S = \rho_w C_{ps} (T_w - T_{eq}) \left[ 1 - \exp\left(-\frac{\tau_f}{\tau_T}\right) \right] \left( \frac{4\pi r_0^3}{3} \frac{dF}{dr_0} \right), \quad (A1)$$

$$Q_L = \begin{cases} \rho_w L_v \left\{ 1 - \left[ \frac{r(\tau_f)}{r_0} \right]^3 \right\} \left( \frac{4\pi r_0^3}{3} \frac{dF}{dr_0} \right), & \tau_f \leq \tau_r, \\ \rho_w L_v \left\{ 1 - \left( \frac{r_{eq}}{r_0} \right)^3 \right\} \left( \frac{4\pi r_0^3}{3} \frac{dF}{dr_0} \right), & \tau_f > \tau_r. \end{cases} \quad (A2)$$

371 Here  $Q_S$ ,  $Q_L$  are sensible heat flux and latent heat flux resulted by sea spray droplets with initial radius  
372  $r_0$ ,  $\rho_w$  is the sea water density,  $C_{ps}$  is the specific heat,  $L_v$  is the latent heat of vaporization of water,  
373  $T_w$  is the water temperature,  $T_{eq}$  is the temperature of droplet when it reaches thermal equilibrium with  
374 ambient condition,  $r_{eq}$  is the radius of droplet when it reaches moisture equilibrium with ambient  
375 condition,  $\tau_f$  is the residence time for droplets in the atmospheric,  $r(\tau_f)$  is the corresponding radius,  
376  $\tau_T$  is the characteristic e-folding time of droplet temperature, and  $\tau_r$  is the characteristic e-folding time  
377 of droplet radius. The detailed calculation of these microphysical quantities can be found in Andreas  
378 (1989, 1990, 1992). And  $dF/dr_0$  is the sea spray generation function, which represents the number  
379 produced of droplets with initial radius  $r_0$  (Andreas, 1992). For this term, the function of Fairall et al.  
380 (1994) was recommended by Andreas (2002). According to the review in Andreas (2002), the  $dF/dr_0$   
381 of Fairall et al. (1994) is related on that of Andreas (1992) as

$$\frac{dF}{dr_0} = 38 \times 3.84 \times 10^{-6} U_{10}^{3.41} r_0^{-0.024} \left. \frac{dF_{A92}}{dr_{80}} \right|_{U_{10}=11 \text{ m/s}}, \quad (A3)$$

$$\left. \frac{dF_{A92}}{dr_{80}} \right|_{U_{10}=11 \text{ m/s}} = \begin{cases} e^{(4.405-2.646(\log r_{80})-3.156(\log r_{80})^2+8.902(\log r_{80})^3-4.482(\log r_{80})^4)}, & r_{80} \leq 15 \mu\text{m}; \\ 1.02 \times 10^4 r_{80}^{-1}, & 15 \leq r_{80} \leq 37.5 \mu\text{m}; \\ 6.95 \times 10^6 r_{80}^{-2.8}, & 37.5 \leq r_{80} \leq 100 \mu\text{m}; \\ 1.75 \times 10^{17} r_{80}^{-8}, & r_{80} \geq 100 \mu\text{m} \end{cases} \quad (A4)$$

382 Here  $U_{10}$  is the 10-m wind,  $r_{80} = 0.518 r_0^{0.976}$ .

383 The total sea spray fluxes are obtained by integrating  $Q_S$  and  $Q_L$  corresponding to all  $r_0$ . Based on  
384 Andreas (1990), the lower and upper limits of  $r_0$  is  $2 \mu\text{m}$  and  $500 \mu\text{m}$ , that is,

$$\overline{Q_S} = \int_2^{500} Q_S(r_0) dr, \quad (A5)$$

$$\overline{Q_L} = \int_2^{500} Q_L(r_0) dr. \quad (A6)$$

385 While  $\overline{Q_S}$  and  $\overline{Q_L}$  are nominal sea spray fluxes but not the actual  $H_{S,SP}$  and  $H_{L,SP}$  (Andreas and  
386 Decosmo, 1999, 2002), because there are interactions between these two terms and the microphysical  
387 functions also lead to uncertainties (Fairall et al., 1994). Therefore,  $\overline{Q_S}$  and  $\overline{Q_L}$  are tuned by non-



388 negative constants  $\alpha$ ,  $\beta$  and  $\gamma$  (Andreas and Decosmo, 2002; Andreas et al., 2008; Andreas et al., 2015;  
 389 Andreas, 2003) as

$$H_{S,SP} = \beta \overline{Q_S} - (\alpha - \gamma) \overline{Q_L}, \quad (\text{A7})$$

$$H_{L,SP} = \alpha \overline{Q_L}. \quad (\text{A8})$$

390 In Eqn. (A8), the  $\alpha$  term indicates the sea spray-mediated latent heat flux from the top of DEL to  
 391 atmosphere. Because the evaporation of droplets absorbs heat, which is provided by sea spray-mediated  
 392 sensible heat (Fairall et al., 1994), the negative  $\alpha$  term appears in Eqn. (A7). Whereas the evaporation  
 393 also cools DEL and thus increases the air-sea temperature difference, therefore it contributes to a positive  
 394  $\gamma$  term in Eqn. (A7). Different values of  $\alpha$ ,  $\beta$  and  $\gamma$  were given in Andreas and Decosmo (2002),  
 395 Andreas (2003), Andreas et al. (2008) and Andreas et al. (2015), to minimize the bias between  
 396 estimations and observations of turbulent heat fluxes measured by eddy correlation. And Andreas et al.  
 397 (2015) validated the most observation data, which are 4000 sets, to derive  $\alpha = 2.46, \beta = 15.15, \gamma =$   
 398  $1.77$ .

## 399 Appendix B

### 400 Fast Algorithm of A15

401 Andreas (2003) and Andreas et al. (2008, 2015) developed a fast algorithm to approximate  $H_{S,SP}$ ,  
 402  $H_{L,SP}$  by a characteristic radius, that is,

$$H_{S,SP} = \beta \overline{Q_S} - (\alpha - \gamma) \overline{Q_L} \approx \rho_w C_{ps} (T_W - T_{eq,100}) V_S(u_*), \quad (\text{B1})$$

$$H_{L,SP} = \alpha \overline{Q_L} \approx \rho_w L_v \left\{ 1 - \left[ \frac{r(\tau_{f,50})}{50 \mu\text{m}} \right]^3 \right\} V_L(u_*). \quad (\text{B2})$$

403 Here  $T_{eq,100}$  is  $T_{eq}$  of droplets with  $r_0=100 \mu\text{m}$ ,  $\tau_{f,50}$  is  $\tau_f$  of droplets with  $r_0=50 \mu\text{m}$ ,  $V_S$  and  
 404  $V_L$  are functions of the bulk friction velocity  $u_*$ . As indicated by Andreas et al. (2008, 2015), the  
 405 characteristic radiuses of  $100 \mu\text{m}$  and  $50 \mu\text{m}$  for sensible and latent heat fluxes are chosen,  
 406 respectively, because  $Q_S$  and  $Q_L$  show a large peak in the vicinity of these values (Fig. 1).  $V_S$  and  $V_L$   
 407 are calculated in Andreas et al. (2015) as

$$V_S = \begin{cases} 3.92 \times 10^{-8}, & 0 \leq u_* \leq 0.1480 \text{ m/s} \\ 5.02 \times 10^{-6} u_*^{2.54}, & u_* \geq 0.1480 \text{ m/s} \end{cases} \quad (\text{B3})$$

$$V_L = \begin{cases} 1.76 \times 10^{-9}, & 0 \leq u_* \leq 0.1358 \text{ m/s} \\ 2.08 \times 10^{-7} u_*^{2.39}, & u_* \geq 0.1358 \text{ m/s} \end{cases} \quad (\text{B4})$$

## 408 Appendix C

### 409 Gaussian Quadrature (GQ)

410 GQ is a method to approximate the definite integral of a function  $f(x)$  via the function values at a  
 411 small number of specified nodes (Gauss, 1815; Jacobi, 1826). In this study we use the form of n-node  
 412 Gauss–Legendre quadrature on  $[-1, 1]$  as

$$\int_{-1}^1 f(x) dx \approx \sum_{i=1}^n \omega_i f(x_i). \quad (\text{C1})$$

413 Here  $x_i$  is the specified node, and  $\omega_i$  is the corresponding weight. For  $n=3$ ,  $x_1=-0.775$ ,  $x_2=0$ ,  
 414  $x_3=0.775$ ,  $\omega_1=\omega_3=0.556$ ,  $\omega_2=0.889$ .

415 While for a function  $g(\xi)$  on  $[a, b]$ , Eqn. (C1) can be transformed to

$$\begin{aligned} \int_a^b g(\xi) d\xi &= \int_{-1}^1 g\left(\frac{b-a}{2}x + \frac{a+b}{2}\right) \frac{d\xi}{dx} dx \\ &\approx \frac{b-a}{2} \sum_{i=1}^n \omega_i g\left(\frac{b-a}{2}x_i + \frac{a+b}{2}\right). \end{aligned} \quad (\text{C2})$$

### 416 Code and data availability

417 The code of sea spray can be found under <https://doi.org/10.5281/zenodo.7100345> or  
 418 <https://zenodo.org/record/7100345#.Y66vRtVByHt> (Shi and Xu, 2022). The code for CFSv2.0-WW3  
 419 system can be found under <https://doi.org/10.5281/zenodo.5811002> (Shi et al., 2021) including the  
 420 coupling, preprocessing, run control and postprocessing scripts. The initial fields for CFSv2.0 are  
 421 generated by the real time operational Climate Data Assimilation System, downloaded from the CFSv2.0  
 422 official website (<http://nomads.ncep.noaa.gov/pub/data/nccf/com/cfs/prod>). The daily average satellite  
 423 Optimum Interpolation SST (OISST) data are obtained from NOAA (<https://www.ncdc.noaa.gov/oisst>).  
 424 The fifth generation European Centre for Medium-Range Weather Forecasts (ECMWF) Reanalysis  
 425 (ERA5) are available at the Copernicus Climate Change Service (C3S) Climate Data Store  
 426 (<https://cds.climate.copernicus.eu/cdsapp#!dataset/reanalysis-era5-single-levels>). The daily Objectively  
 427 Analyzed air-sea Fluxes (OAFflux) products are available at <https://oafux.whoi.edu/heat-flux>. The global  
 428 monthly mean salinity observations of European Space Agency (ESA) are from <https://climate.esa.int>.

429 The monthly global ocean RSS Satellite Data Products for 10-m wind speed are from  
430 [https://data.remss.com/wind/monthly\\_1deg/](https://data.remss.com/wind/monthly_1deg/), and the Reprocessed L4 Satellite Measurements for  
431 significant wave height are from <https://doi.org/10.48670/moi-00177>.

#### 432 **Author contribution**

433 FX and RS designed the experiments and RS carried them out. RS developed the code of coupling  
434 parametrizations and produced the figures. RS prepared the manuscript with contributions from all co-  
435 authors. FX contributed to review and editing.

#### 436 **Acknowledgments**

437 This work was supported by the National Key Research and Development Program of China  
438 (2020YFA0607900, 2021YFC3101601), and the National Natural Science Foundation of China  
439 (42176019). We thank Dr. Jiangnan Li for help of GQ codes. We also thank two anonymous reviewers  
440 and the handling editor for their constructive comments.

#### 441 **Competing Interests**

442 The contact author has declared that neither they nor their co-authors have any competing interests.

#### 443 **References**

444 Accadia, C., Zecchetto, S., Lavagnini, A., and Speranza, A.: Comparison of 10-m wind forecasts from a  
445 regional area model and QuikSCAT scatterometer wind observations over the Mediterranean Sea, *Mon.*  
446 *Weather Rev.*, 135, 1945-1960, 2007.

447 Alessandro, J. D., Diao, M., Wu, C., Liu, X., Jensen, J. B., and Stephens, B. B.: Cloud phase and relative  
448 humidity distributions over the Southern Ocean in austral summer based on in situ observations and  
449 CAM5 simulations, *Journal of Climate*, 32, 2781-2805, 2019.

450 Andreas, E. L.: Thermal and size evolution of sea spray droplets, 1989.

451 Andreas, E. L.: Time constants for the evolution of sea spray droplets, *Tellus B*, 42, 481-497, 1990.

452 Andreas, E. L.: Sea spray and the turbulent air - sea heat fluxes, *Journal of Geophysical Research*:

453 Oceans, 97, 11429-11441, 1992.

454 Andreas, E. L.: A new sea spray generation function for wind speeds up to 32 ms<sup>-1</sup>, Journal of Physical  
455 Oceanography, 28, 2175-2184, 1998.

456 Andreas, E. L.: A review of the sea spray generation function for the open ocean, Advances in Fluid  
457 Mechanics, 33, 1-46, 2002.

458 Andreas, E. L.: 3.4 AN ALGORITHM TO PREDICT THE TURBULENT AIR-SEA FLUXES IN  
459 HIGH-WIND, SPRAY CONDITIONS, 2003.

460 Andreas, E. L.: Spray stress revisited, Journal of physical oceanography, 34, 1429-1440, 2004.

461 Andreas, E. L.: Spray-mediated enthalpy flux to the atmosphere and salt flux to the ocean in high winds,  
462 Journal of physical oceanography, 40, 608-619, 2010.

463 Andreas, E. L. and Decosmo, J.: Sea spray production and influence on air-sea heat and moisture fluxes  
464 over the open ocean, in: Air-sea exchange: physics, chemistry and dynamics, Springer, 327-362, 1999.

465 Andreas, E. L. and Decosmo, J.: The signature of sea spray in the HEXOS turbulent heat flux data,  
466 Boundary-layer meteorology, 103, 303-333, 2002.

467 Andreas, E. L. and Emanuel, K. A.: Effects of sea spray on tropical cyclone intensity, Journal of the  
468 atmospheric sciences, 58, 3741-3751, 2001.

469 Andreas, E. L., Mahrt, L., and Vickers, D.: An improved bulk air - sea surface flux algorithm, including  
470 spray - mediated transfer, Quarterly Journal of the Royal Meteorological Society, 141, 642-654, 2015.

471 Andreas, E. L., Persson, P. O. G., and Hare, J. E.: A bulk turbulent air-sea flux algorithm for high-wind,  
472 spray conditions, Journal of Physical Oceanography, 38, 1581-1596, 2008.

473 Andreas, E. L., Edson, J. B., Monahan, E. C., Rouault, M. P., and Smith, S. D.: The spray contribution  
474 to net evaporation from the sea: A review of recent progress, Boundary-Layer Meteorology, 72, 3-52,  
475 1995.

476 Bao, Y., Song, Z., and Qiao, F.: FIO - ESM version 2.0: Model description and evaluation, Journal of  
477 Geophysical Research: Oceans, 125, e2019JC016036, 2020.

478 Bodas-Salcedo, A., Williams, K., Field, P., and Lock, A.: The surface downwelling solar radiation  
479 surplus over the Southern Ocean in the Met Office model: The role of midlatitude cyclone clouds, Journal  
480 of Climate, 25, 7467-7486, 2012.

481 Borisenkov, E.: Some mechanisms of atmosphere-ocean interaction under stormy weather conditions,  
482 *Probl Arct Antarct*, 43, 73-83, 1974.

483 Bortkovskii, R.: On the mechanism of interaction between the ocean and the atmosphere during a storm,  
484 *Fluid Mech Sov Res*, 2, 87-94, 1973.

485 Burk, S. D.: The generation, turbulent transfer and deposition of the sea-salt aerosol, *Journal of*  
486 *Atmospheric Sciences*, 41, 3040-3051, 1984.

487 Ceppi, P., Hwang, Y. T., Frierson, D. M., and Hartmann, D. L.: Southern Hemisphere jet latitude biases  
488 in CMIP5 models linked to shortwave cloud forcing, *Geophysical Research Letters*, 39, 2012.

489 Djurdjevic, V. and Rajkovic, B.: Verification of a coupled atmosphere-ocean model using satellite  
490 observations over the Adriatic Sea, *Annales Geophysicae*, 1935-1954,

491 Edson, J. B. and Andreas, E. L.: Modeling the role of sea spray on air-sea heat and moisture exchange,  
492 *Final Rep*, 6, 18, 1997.

493 Emanuel, K. A.: Sensitivity of tropical cyclones to surface exchange coefficients and a revised steady-  
494 state model incorporating eye dynamics, *Journal of Atmospheric Sciences*, 52, 3969-3976, 1995.

495 Fairall, C. and Larsen, S. E.: Dry deposition, surface production and dynamics of aerosols in the marine  
496 boundary layer, *Atmospheric Environment (1967)*, 18, 69-77, 1984.

497 Fairall, C., Davidson, K., and Schacher, G.: An analysis of the surface production of sea - salt aerosols,  
498 *Tellus B*, 35, 31-39, 1983.

499 Fairall, C., Kepert, J., and Holland, G.: The effect of sea spray on surface energy transports over the  
500 ocean, *Global Atmos. Ocean Syst*, 2, 121-142, 1994.

501 Fairall, C., Bradley, E. F., Rogers, D. P., Edson, J. B., and Young, G. S.: Bulk parameterization of air -  
502 sea fluxes for tropical ocean - global atmosphere coupled - ocean atmosphere response experiment,  
503 *Journal of Geophysical Research: Oceans*, 101, 3747-3764, 1996.

504 Fox-Kemper, B., Johnson, L., and Qiao, F.: Ocean near-surface layers, in: *Ocean Mixing*, Elsevier, 65-  
505 94, 2022.

506 Garg, N., Ng, E. Y. K., and Narasimalu, S.: The effects of sea spray and atmosphere-wave coupling on  
507 air-sea exchange during a tropical cyclone, *Atmospheric Chemistry and Physics*, 18, 6001-6021, 2018.

508 Gauss, C. F.: *Methodvs nova integralivm valores per approximationem inveniendi, apvd Henricvm*

509 Dieterich1815.

510 Griffies, S. M., Harrison, M. J., Pacanowski, R. C., and Rosati, A.: A technical guide to MOM4, GFDL  
511 Ocean Group Tech. Rep, 5, 342, 2004.

512 WAVEWATCH III Development Group: User manual and system documentation of WAVEWATCH  
513 III version 5.16, NOAA/NWS/NCEP/MMAB Technical Note 329, 326, 2016.

514 Hersbach, H., Bell, B., Berrisford, P., Hirahara, S., Horányi, A., Muñoz - Sabater, J., Nicolas, J., Peubey,  
515 C., Radu, R., and Schepers, D.: The ERA5 global reanalysis, Quarterly Journal of the Royal  
516 Meteorological Society, 146, 1999-2049, 2020.

517 Jacobi, C. G. J.: Ueber Gauss neue Methode, die Werthe der Integrale näherungsweise zu finden, 1826.

518 Kalnay, E., Kanamitsu, M., Kistler, R., Collins, W. D., Deaven, D. G., Gandin, L. S., Iredell, M. D., Saha,  
519 S., White, G. H., and Woollen, J.: The NCEP/NCAR 40-Year Reanalysis Project, Bulletin of the  
520 American Meteorological Society, 77, 437-471, [http://dx.doi.org/10.1175/1520-  
521 0477\(1996\)077%3C0437:TNYRP%3E2.0.CO;2](http://dx.doi.org/10.1175/1520-0477(1996)077%3C0437:TNYRP%3E2.0.CO;2), 1996.

522 Koga, M.: Direct production of droplets from breaking wind - waves—its observation by a multi -  
523 colored overlapping exposure photographing technique, Tellus, 33, 552-563, 1981.

524 Lhuissier, H. and Villermaux, E.: Bursting bubble aerosols, Journal of Fluid Mechanics, 696, 5-44, 2012.

525 Li, J., Waliser, D., Stephens, G., Lee, S., L'Ecuyer, T., Kato, S., Loeb, N., and Ma, H. Y.: Characterizing  
526 and understanding radiation budget biases in CMIP3/CMIP5 GCMs, contemporary GCM, and reanalysis,  
527 Journal of Geophysical Research: Atmospheres, 118, 8166-8184, 2013.

528 Li, J. N. and Barker, H. W.: Computation of domain - average radiative flux profiles using Gaussian  
529 quadrature, Quarterly Journal of the Royal Meteorological Society, 144, 720-734, 2018.

530 Lindemann, D., Avila-Diaz, A., Pezzi, L., Rodrigues, J., Freitas, R. A., Coelho, L., Alonso, M., and  
531 Cerón, W. L.: The Surface Wind Influence on the Heat Fluxes Variability on the South Atlantic, 2021.

532 Ling, S. and Kao, T.: Parameterization of the moisture and heat transfer process over the ocean under  
533 whitecap sea states, Journal of Physical Oceanography, 6, 306-315, 1976.

534 Liu, B., Guan, C., Xie, L. a., and Zhao, D.: An investigation of the effects of wave state and sea spray on  
535 an idealized typhoon using an air-sea coupled modeling system, Advances in Atmospheric Sciences, 29,  
536 391-406, 2012.

537 Liu, L., Zhang, C., Li, R., and Wang, B.: C-Coupler2: a flexible and user-friendly community coupler  
538 for model coupling and nesting, *Geoscientific Model Development Discussions*, 11, 1-63,  
539 <http://dx.doi.org/10.5194/gmd-11-3557-2018>, 2018.

540 McClarren, R.: Gauss Quadrature and Multi-dimensional Integrals, *Computational Nuclear Engineering  
541 and Radiological Science Using Python*; Academic Press: Cambridge, MA, USA, 287-299, 2018.

542 Melville, W. K.: *The role of surface-wave breaking in air-sea interaction*, 1996.

543 Monahan, E. and Van Patten, M. A.: *The climate and health implications of bubble-mediated sea-air  
544 exchange*, 1988.

545 Monahan, E., Davidson, K., and Spiel, D.: Whitecap aerosol productivity deduced from simulation tank  
546 measurements, *Journal of Geophysical Research: Oceans*, 87, 8898-8904, 1982.

547 Myslenkov, S., Zelenko, A., Resnyanskii, Y., Arkhipkin, V., and Silvestrova, K.: Quality of the Wind  
548 Wave Forecast in the Black Sea Including Storm Wave Analysis, *Sustainability*, 13, 13099, 2021.

549 Pruppacher, H. R. and Klett, J. D.: Microstructure of atmospheric clouds and precipitation, in:  
550 *Microphysics of Clouds and Precipitation*, Springer, 9-55, 1978.

551 Resch, F. and Afeti, G.: Film drop distributions from bubbles bursting in seawater, *Journal of  
552 Geophysical Research: Oceans*, 96, 10681-10688, 1991.

553 Reynolds, R. W., Smith, T. M., Liu, C., Chelton, D. B., Casey, K. S., and Schlax, M. G.: Daily high-  
554 resolution-blended analyses for sea surface temperature, *Journal of climate*, 20, 5473-5496, 2007.

555 Saha, S., Moorthi, S., Wu, X., Wang, J., Nadiga, S., Tripp, P., Behringer, D., Hou, Y., Chuang, H., and  
556 Iredell, M. D.: The NCEP Climate Forecast System Version 2, *Journal of Climate*, 27, 2185-2208,  
557 <http://dx.doi.org/10.1175/JCLI-D-12-00823.1>, 2014.

558 Seethala, C., Zuidema, P., Edson, J., Brunke, M., Chen, G., Li, X. Y., Painemal, D., Robinson, C.,  
559 Shingler, T., and Shook, M.: On assessing ERA5 and MERRA2 representations of cold - air outbreaks  
560 across the Gulf Stream, *Geophysical research letters*, 48, e2021GL094364, 2021.

561 Shi, R., Xu, F., Liu, L., Fan, Z., Yu, H., Li, H., Li, X., and Zhang, Y.: The effects of ocean surface waves  
562 on global intraseasonal prediction: case studies with a coupled CFSv2. 0–WW3 system, *Geoscientific  
563 Model Development*, 15, 2345-2363, 2022.

564 Smith, R. K.: On the theory of CISK, *Quarterly Journal of the Royal Meteorological Society*, 123, 407-

565 418, 1997.

566 Song, Y., Qiao, F., Liu, J., Shu, Q., Bao, Y., Wei, M., and Song, Z.: Effects of sea spray on large-scale  
567 climatic features over the Southern Ocean, *Journal of Climate*, 1-51, 2022.

568 Spiel, D. E.: More on the births of jet drops from bubbles bursting on seawater surfaces, *Journal of*  
569 *Geophysical Research: Oceans*, 102, 5815-5821, 1997.

570 Thorpe, S.: Bubble clouds and the dynamics of the upper ocean, *Quarterly Journal of the Royal*  
571 *Meteorological Society*, 118, 1-22, 1992.

572 Troitskaya, Y., Kandaurov, A., Ermakova, O., Kozlov, D., Sergeev, D., and Zilitinkevich, S.: The “bag  
573 breakup” spume droplet generation mechanism at high winds. Part I: Spray generation function, *Journal*  
574 *of physical oceanography*, 48, 2167-2188, 2018.

575 Van Eijk, A., Kusmierczyk - Michulec, J., Francius, M., Tedeschi, G., Piazzola, J., Merritt, D., and  
576 Fontana, J.: Sea - spray aerosol particles generated in the surf zone, *Journal of Geophysical Research:*  
577 *Atmospheres*, 116, 2011.

578 Veron, F.: Ocean spray, *Annu. Rev. Fluid Mech*, 47, 507-538, 2015.

579 Wang, C., Zhang, L., Lee, S.-K., Wu, L., and Mechoso, C. R.: A global perspective on CMIP5 climate  
580 model biases, *Nature Climate Change*, 4, 201-205, 2014.

581 Wu, J.: Evaporation due to spray, *Journal of Geophysical Research*, 79, 4107-4109, 1974.

582 Wu, L., Cheng, X., Zeng, Q., Jin, J., Huang, J., and Feng, Y.: On the upward flux of sea - spray spume  
583 droplets in high - wind conditions, *Journal of Geophysical Research: Atmospheres*, 122, 5976-5987,  
584 2017.

585 Xu, X., Voermans, J., Ma, H., Guan, C., and Babanin, A. V.: A Wind-Wave-Dependent Sea Spray  
586 Volume Flux Model Based on Field Experiments, *Journal of Marine Science and Engineering*, 9, 1168,  
587 2021a.

588 Xu, X., Voermans, J., Liu, Q., Moon, I.-J., Guan, C., and Babanin, A.: Impacts of the Wave-Dependent  
589 Sea Spray Parameterizations on Air-Sea-Wave Coupled Modeling under an Idealized Tropical Cyclone,  
590 *Journal of Marine Science and Engineering*, 9, 1390, 2021b.

591 Yu, L., Jin, X., and Weller, R. A.: 2008: Multidecade global flux datasets from the Objectively Analyzed  
592 Air-Sea Fluxes (OAFlux) Project: Latent and sensible heat fluxes, ocean evaporation, and related surface



593 meteorological variables. Woods Hole Oceanographic Institution OAFlux Project Tec, Rep,  
594 Zhao, B., Qiao, F., Cavaleri, L., Wang, G., Bertotti, L., and Liu, L.: Sensitivity of typhoon modeling to  
595 surface waves and rainfall, *Journal of Geophysical Research: Oceans*, 122, 1702-1723, 2017.  
596  
597

**Table 1.** The runtime of CFSv2.0-WW3 global experiments for 7-day forecast with different parameterizations.

<b>7-day Forecast</b>	<b>Runtime (h)</b>
SPRAY-A92	126.94
SPRAY-A15	7.60
SPRAY-GQ	7.67

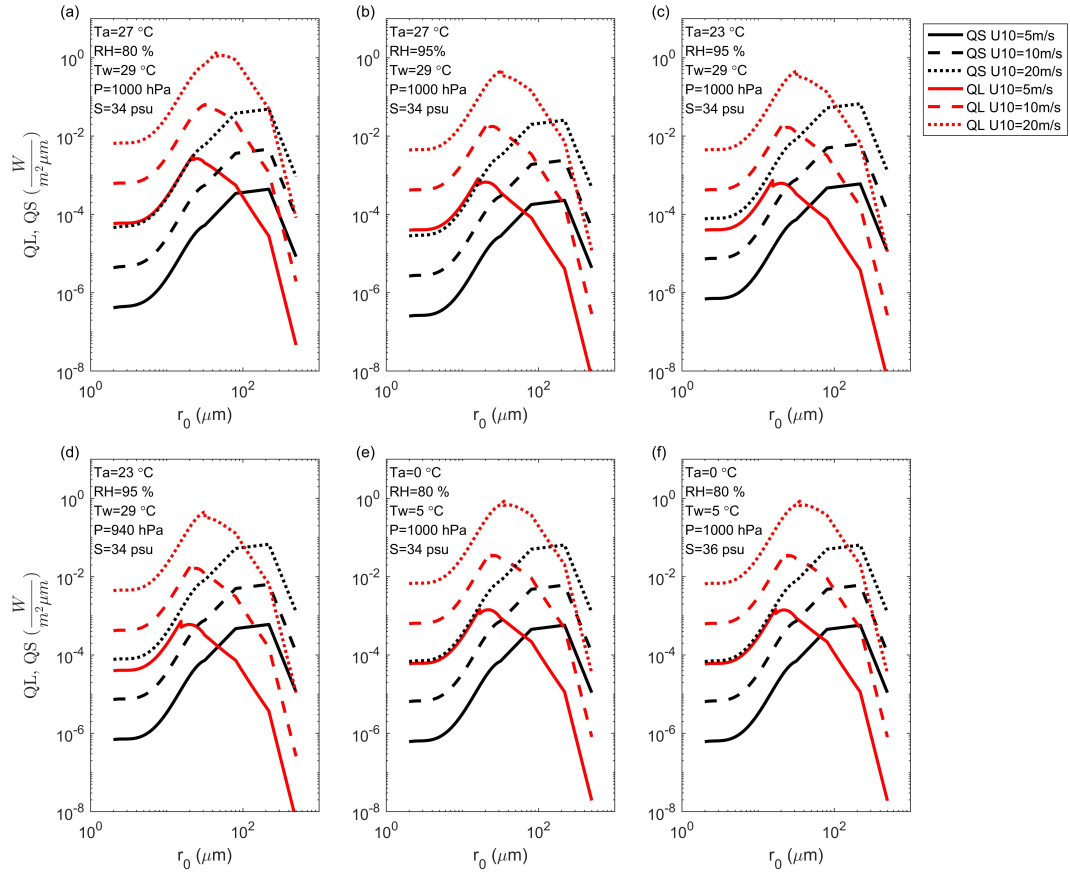


**Figure 1.** The radius-specific sea spray-mediated sensible ( $Q_S$ ; black) and latent ( $Q_L$ ; red) heat fluxes as functions of initial radius  $r_0$ :  $U_{10}$ ,  $T_a$ ,  $RH$ ,  $T_w$ ,  $P$  and  $S$  are 10-m wind speed, 2-m air temperature, 2-m relative humidity, sea surface temperature, surface air pressure and surface salinity, respectively.

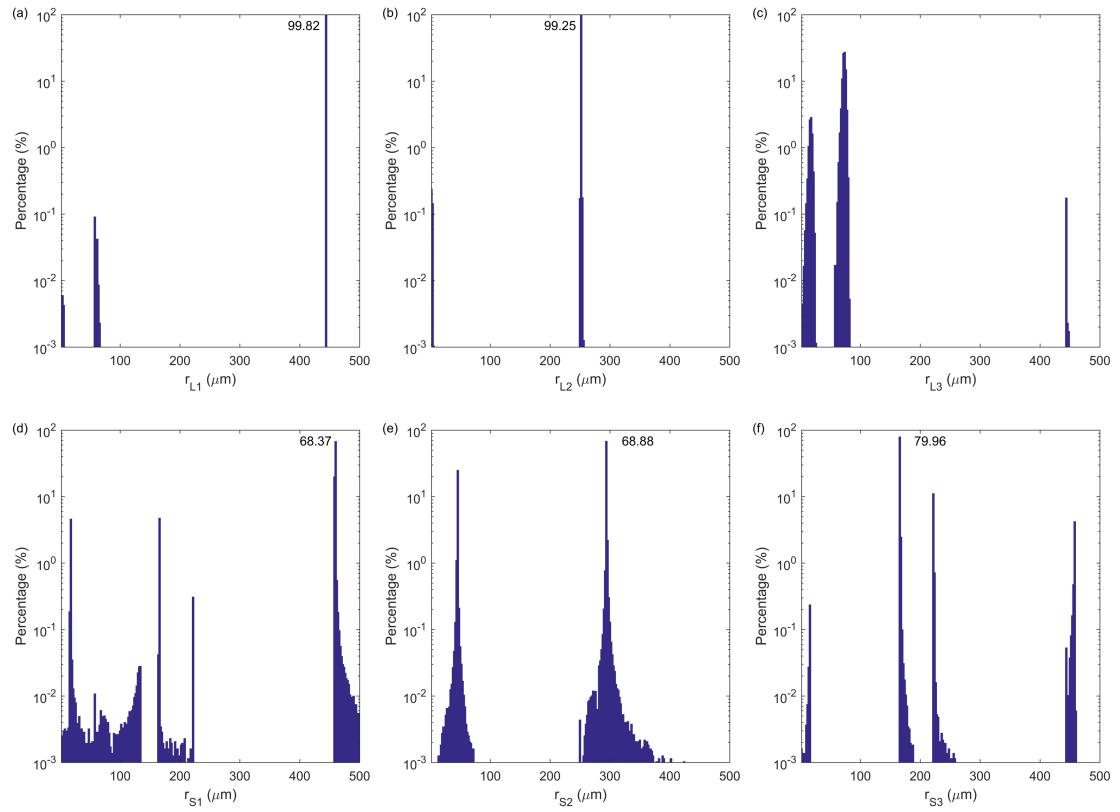


**Figure 2.** The distribution of occurrence frequency in percentage for GQ radius nodes: (a) the first node of latent heat flux; (b) the second node of latent heat flux; (c) the third node of latent heat flux; (d) the first node of sensible heat flux; (e) the second node of sensible heat flux; (f) the third node of sensible heat flux. The peak frequencies are marked.

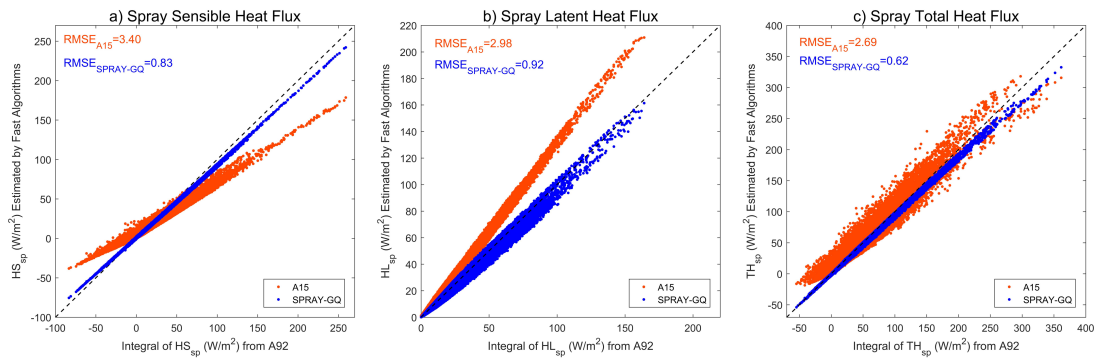


**Figure 3.** Scatter plots of  $H_{S,SP}$  (a),  $H_{L,SP}$  (b) and total heat flux  $TH_{SP} = H_{S,SP} + H_{L,SP}$  (c) estimated by fast algorithms (y-axis) vs those estimated by spectral integral in microphysical parameterization (x-axis): The dotted black line is  $y=x$ . The corresponding RMSEs are marked in the upper left corner.

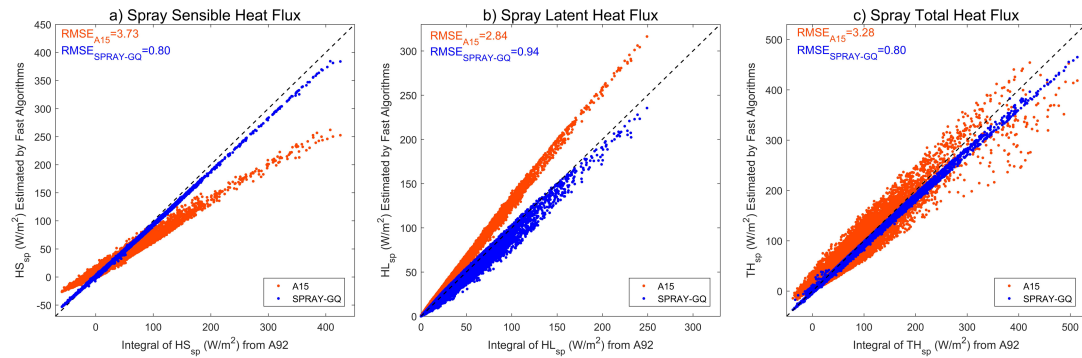


**Figure 4.** The same as Figure 3, but WSP10, 2-m air temperature and 2-m specific humidity of OAF flux are used.

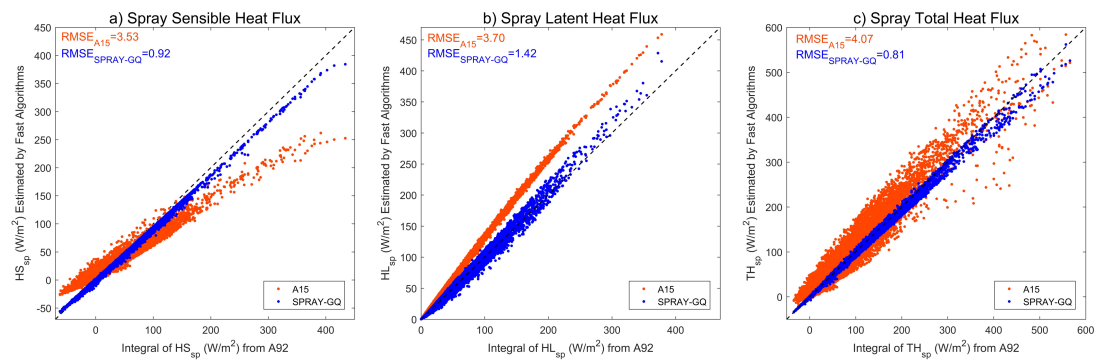


**Figure 5.** The same as Figure 4, but SWH is derived by WSP10 instead of ERA5 SWH.

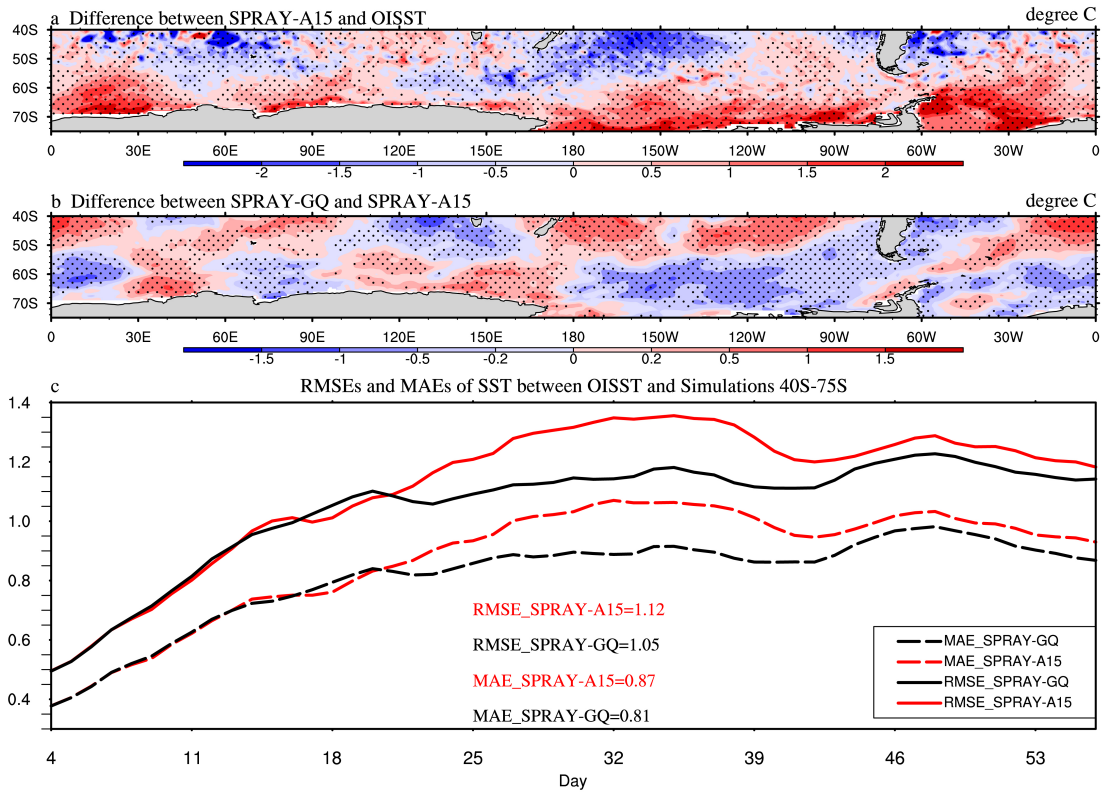


**Figure 6.** The 53-day average SST ( $^{\circ}\text{C}$ ) differences between SPRAY-A15 and OISST (a; SPRAY-A15 minus OISST), the differences between SPRAY-GQ and SPRAY-A15 (b; SPRAY-GQ minus SPRAY-A15), and the time series of domain-averaged RMSE and MAE (c; 0-360 $^{\circ}\text{E}$ , 40-75 $^{\circ}\text{S}$ ) in Jan-Feb, 2017. The first 3-day simulation is discarded. The dotted areas are statistically significant at 95% confidence level.

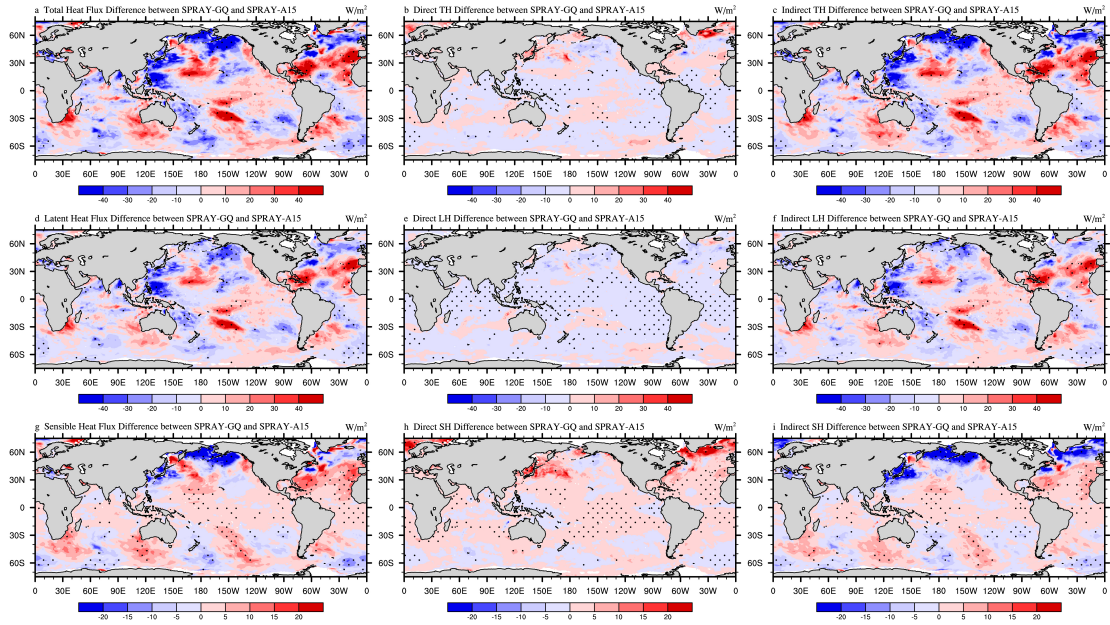


**Figure 7.** The 53-day average differences of total heat flux (a-c), latent heat flux (d-f), and sensible heat flux (g-i) between SPRAY-GQ and SPRAY-A15 (SPRAY-GQ minus SPRAY-A15) in Jan-Feb, 2017. The direct differences indicate sea spray-mediated heat flux differences (b, e, h), and the indirect differences indicate interfacial (bulk) heat flux differences resulted by sea spray (c, f, i). The dotted areas are statistically significant at 95% confidence level. A positive value of flux indicates an upward direction.

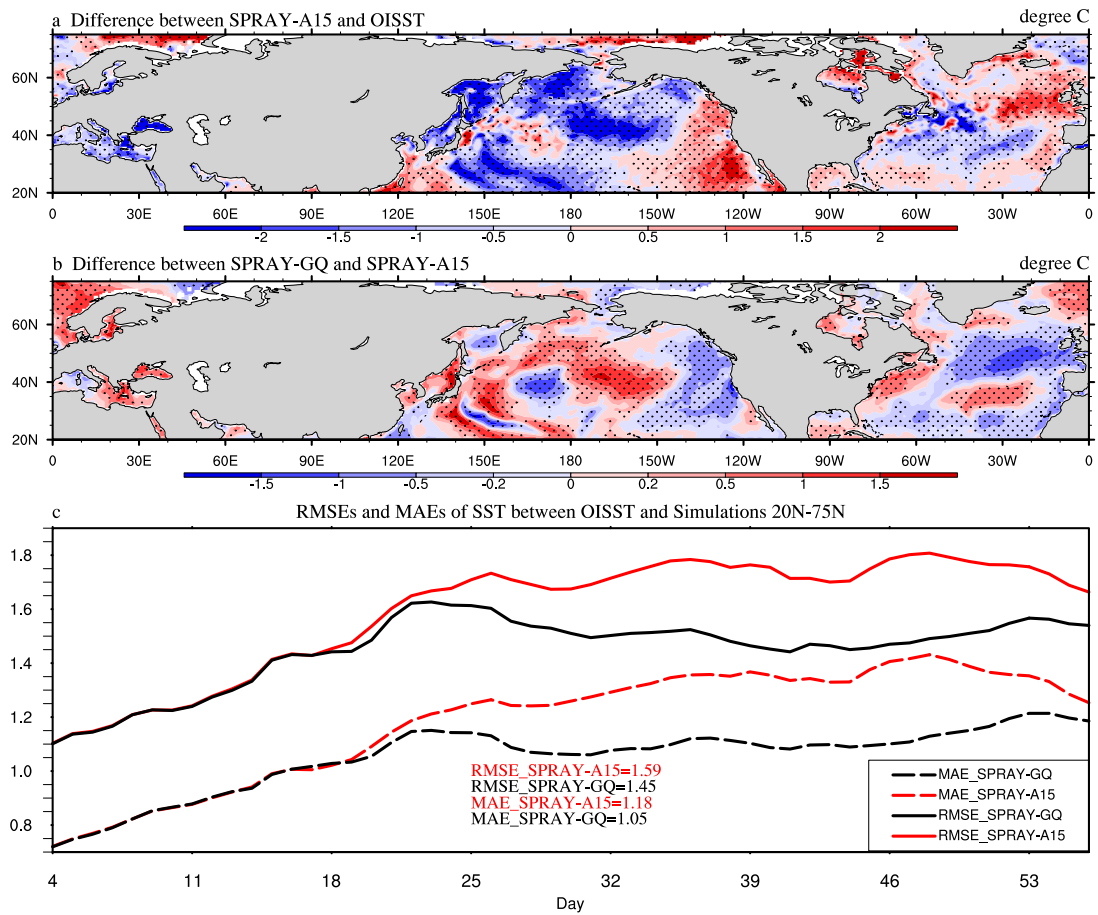


**Figure 8.** The same as Figure 6, but for Aug-Sep, 2018 in 0-360°E, 20-75°N.



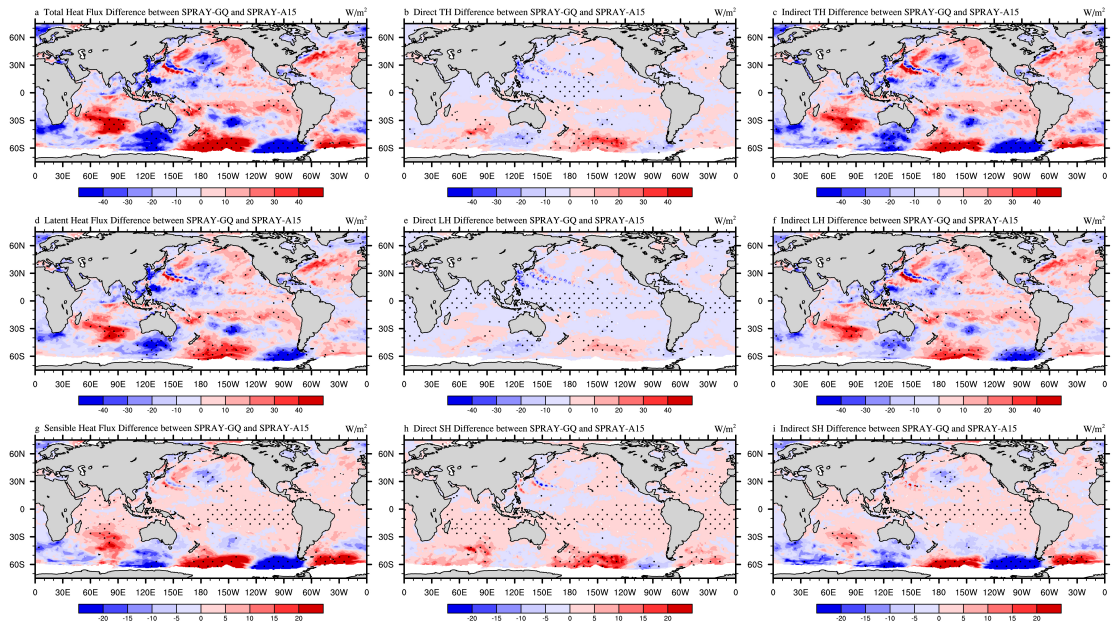
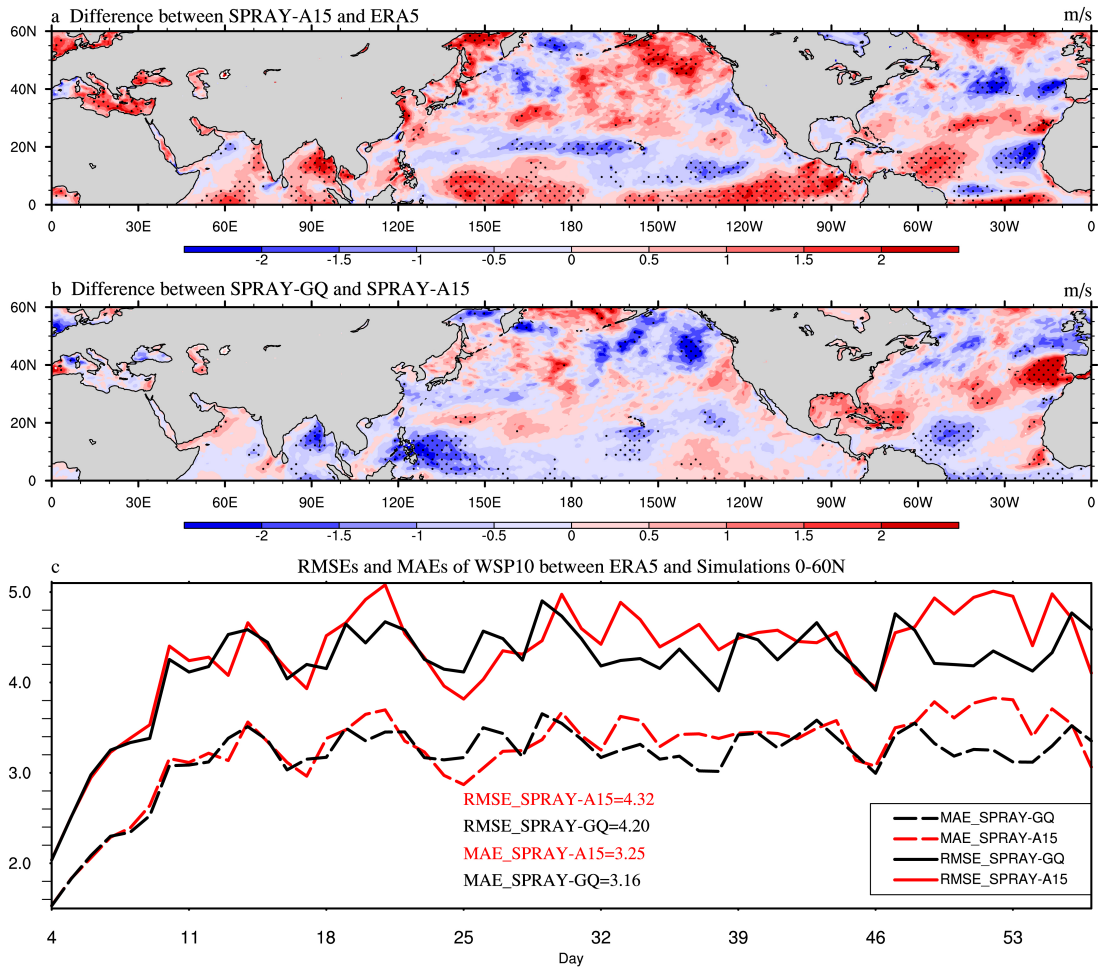
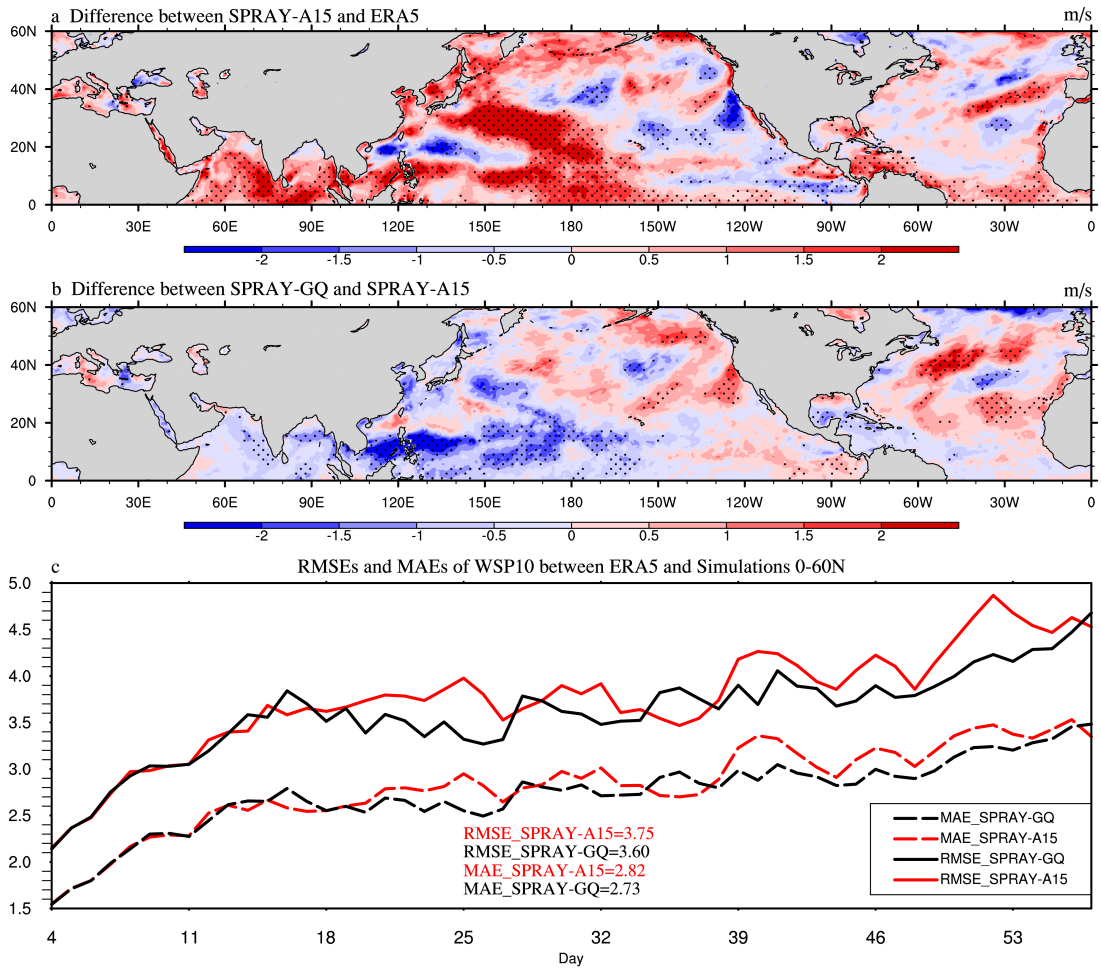


Figure 9. The same as Figure 7, but for Aug-Sep, 2018.



**Figure 10.** The 53-day average WSP10 (m/s) differences between SPRAY-A15 and ERA5 (a; SPRAY-A15 minus ERA5), the differences between SPRAY-GQ and SPRAY-A15 (b; SPRAY-GQ minus SPRAY-A15), and the time series of domain-averaged RMSE and MAE (c; 0-360°E, 0-60°N) in Jan-Feb, 2017. The first 3-day simulation is discarded. The dotted areas are statistically significant at 95% confidence level.



**Figure 11.** The same as Figure 10, but for Aug-Sep, 2018.

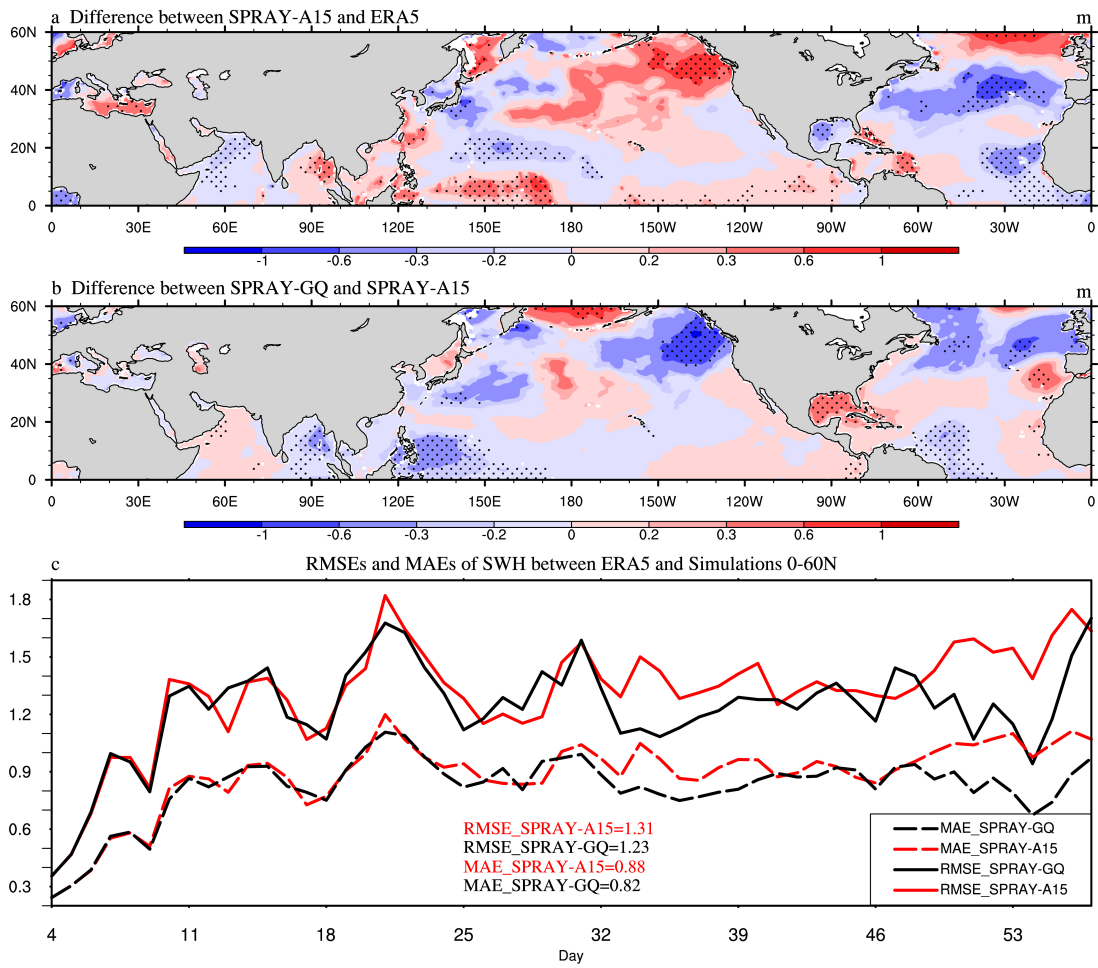


**Figure 12.** The 53-day average SWH (m) differences between SPRAY-A15 and ERA5 (a; SPRAY-A15 minus ERA5), the differences between SPRAY-GQ and SPRAY-A15 (b; SPRAY-GQ minus SPRAY-A15), and the time series of domain-averaged RMSE and MAE (c; 0-360°E, 0-60°N) in Jan-Feb, 2017. The first 3-day simulation is discarded. The dotted areas are statistically significant at 95% confidence level.

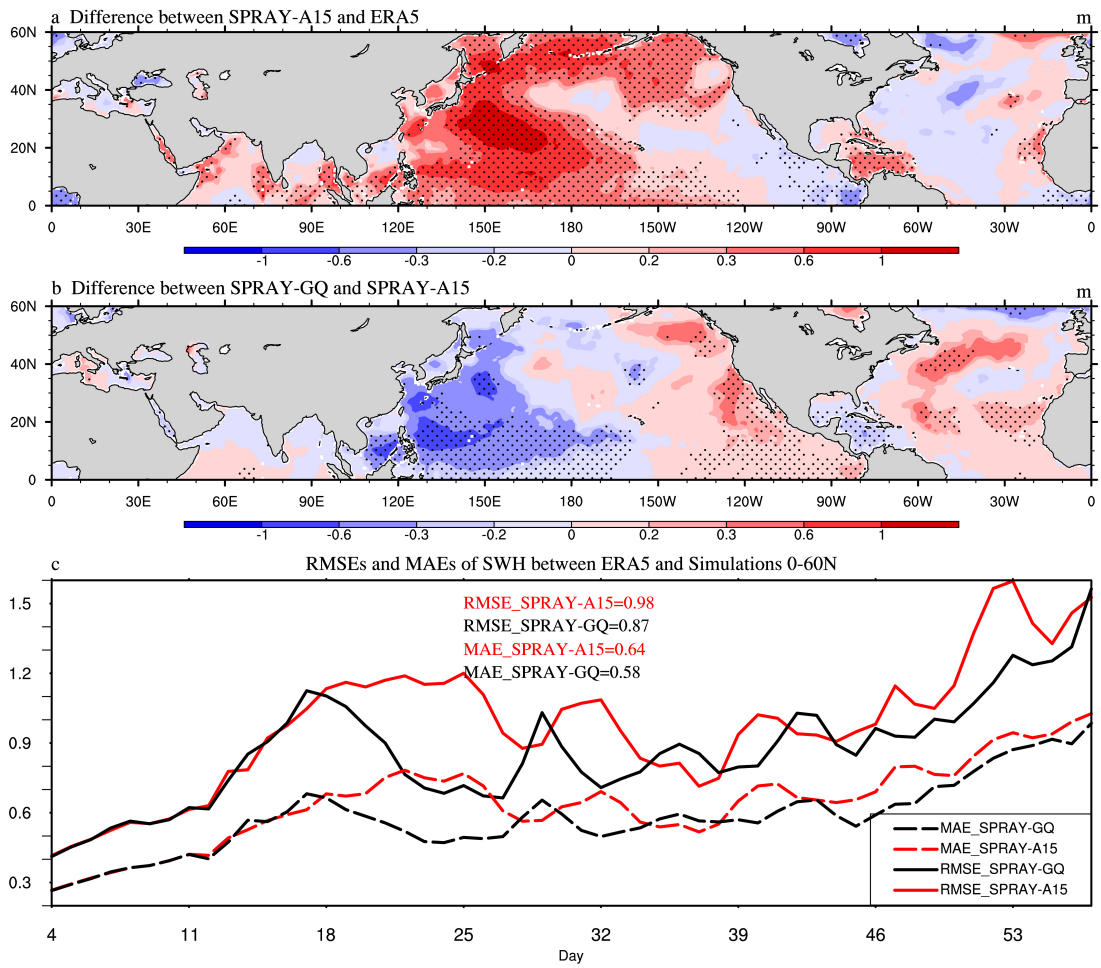


**Figure 13.** The same as Figure 12, but for Aug-Sep, 2018.